VII International Conference on Computational Methods in Marine Engineering
MARINE 2017
M. Visonneau, P. Queutey and D. Le Touzé (Eds)

MARINE CYCLOIDAL PROPULSION MODELLING FOR DP APPLICATIONS

MARCO ALTOSOLE[*], SILVIA DONNARUMMA[†], VALENTINA SPAGNOLO[‡] AND STEFANO VIGNOLO[‡]

* Department of Electrical, Electronic, Telecommunications Engineering and Naval Architecture (DITEN)
Polytechnic School of Genoa University, Italy
Via all'Opera Pia 11A, 16145 Genova, Italy
e-mail: marco.altosole@unige.it

‡ Department of Mechanical, Energy, Management and Transport Engineering (DIME)
Polytechnic School of Genoa University
Via all'Opera Pia 15, 16145 Genova, Italy
e-mail:spagnolo.v86@gmail.it, vignolo@dime.unige.it

† Department of Industrial Engineering (DII)
University of Trento
Via Sommarive 9, 38123 Povo (TN)
e-mail : silvia.donnarumma@unitn.it

Key words: cycloidal propeller, dynamic positioning systems, simulation

Abstract. This paper presents the numerical modelling of a cycloidal propeller in free-running conditions together with its possible applications. The model calibration is carried out by comparing simulation results with experimental data of an existing cycloidal unit. The achieved results support the main strength of the proposed simulation approach: propeller fluid dynamics is not calculated, avoiding demanding computations that would not allow an effective simulation of the whole propulsion plant. As a case study, the cycloidal propulsors model is used for the thruster allocation assessment of the Dynamic Positioning (DP) system of a surface vessel, originally equipped with traditional propellers. Then, the steady-state performance analysis of the DP system is carried out in terms of a comparison between the two distinct propulsion configurations.

1 INTRODUCTION

Cycloidal propellers are able to provide thrust by rotating and additionally oscillating blades. They are classified into three main types: true cycloidal (e.g. Kirstem Boeing Propeller), epicycloidal (e.g. Voith Schneider Propeller) and trochoidal propellers (e.g. Whale Tail Wheel Propeller). The different types of cycloidal propellers are defined by their eccentricity value e, i.e. the ratio between the distance of the steering center from the propeller axis, and the radius of the orbit which defines the position of the blade axes. According to this definition [1], an epicycloidal propeller has $e < 1$, a true cycloidal propeller is characterized by $e = 1$ and a throcoidal propeller has $e > 1$.

The numerical modelling described in the present study is referred to epicycloidal propulsors. The propeller thrust and torque modelling is based on the kinematical aspects of the blades motion, taking into account suitable correction factors in order to properly consider "dissipative" phenomena such as: interference between blades, the shielding induced by the half of the rotor which receives the incoming flow, and the slight reduction of the reverse thrust. The calibration of the simulator is carried out by comparing simulation results with experimental ones, pertinent to an existing cycloidal unit. The main strength of the proposed simulation approach is from not having to calculate the propeller fluid dynamics, avoiding demanding computations that would not allow an effective simulation of the whole propulsion plant. CFD codes are usually useful for the blade design and then they are mainly used by manufacturers (e.g. a RANS equation code has been used by Voith Schneider to represent the behavior of their epicycloidal propellers [2]), while for other applications simplified approaches can be often more suitable, because able to represent the overall performance of the propeller starting from a very few input data and with a reduced computation time. Similar performance prediction methods are commonly used for traditional marine propellers (e.g. systematic propeller series) and waterjets [3]. On the contrary, in the case of cycloidal propellers, manufacturers do not publicly share their performance maps for confidential reasons, and then simplified simulation approaches are more difficult to be developed. The present simulation method is based on a mixture of theoretical and empirical considerations, as already proposed, although in a very different way, by Taniguchi [4]. In the latter, the total thrust and torque of the propeller are evaluated by integrating the lift and drag forces acting on each blade section and a correction factor is introduced to consider non-uniformity of induced velocity over the blade length.

As an application of the proposed method, the authors discuss different thrust allocation logics of a dynamic positioning (DP) system for a surface vessel, equipped with two cycloidal propellers and a single bow thruster. The examined ship is the same for which a DP system, characterized by a conventional twin-screw propulsion, was already developed and installed on board [5].

1 CYCLOIDAL PROPELLER KINEMATICS

2.1 Kinematical model

In this section, the kinematical model describing the motion of each blade of the cycloidal propeller is presented. For simplicity, a two dimensional plane model is adopted, where two distinguished reference frames are introduced: the first one $(O, \underline{b}_1, \underline{b}_2, \underline{b}_3)$ is fixed to the hull and it has its origin O at the center of the rotor, the unit vector $\underline{b}_1$ points towards the bow, the unit vector $\underline{b}_2$ points towards starboard and the unit vector $\underline{b}_3 = \underline{b}_1 \wedge \underline{b}_2$ points downwards; the second one $(O, \underline{e}_1, \underline{e}_2, \underline{e}_3)$ rotates clockwise about the vertical axis passing through O and parallel to $\underline{b}_3 = \underline{e}_3$, by an angle $\beta \epsilon [0, 2\pi]$ which determines (the perpendicular of) the steering force direction. The angle β is then related to the rudder pitch of the cycloidal propeller. The steering center C lies on the straight line passing through O and parallel to $\underline{e}_2$. The linear transformation between the bases $\{\underline{b}_i\}$ and $\{\underline{e}_i\}$ is expressed as

$$\begin{cases} \underline{e}_1 = \cos\beta\,\underline{b}_1 + \sin\beta\,\underline{b}_2 \\ \underline{e}_2 = -\sin\beta\,\underline{b}_1 + \cos\beta\,\underline{b}_2 \\ \underline{e}_3 = \underline{b}_3 \end{cases} \tag{1}$$

During the revolution motion, the projection P of the blade shaft on the plane $\langle O, \underline{b}_1, \underline{b}_2 \rangle$ describes a circumference having center O and radius R coinciding with the rotor radius. In Cartesian coordinates associated with the frame $\left(O, \underline{b}_1, \underline{b}_2, \underline{b}_3\right)$, such a circumference is parameterized by

$$P(\theta): \begin{cases} x = R\cos\theta \\ y = R\sin\theta \\ z = 0 \end{cases} \tag{2}$$

where θ denotes the angle (function of time) describing the revolution motion of the blade. In the vector basis $\{\underline{b}_i\}$, the unit vector $\underline{t}$ tangent to the circular path of P has components of the form

$$\underline{t}(\theta) = \begin{cases} t_1 = -sin\theta \\ t_2 = +cos\theta \\ t_3 = 0 \end{cases} \tag{3}$$

Introducing the vector

$$(C - O) = s\underline{e}_2 = -s\sin\beta\ \underline{b}_1 + s\cos\beta\,\underline{b}_2 \qquad s \in [0, 0.8R] \tag{4}$$

the vector joining the steering centre C with the point P can be expressed as

$$(P - C) = (R\cos\theta + s\sin\beta)\underline{b}_1 + (R\sin\theta - s\cos\beta)\underline{b}_2 \tag{5}$$

The variable s is usually called driving pitch and it controls thrust magnitude. The unit vector orthogonal to $(P - C)$ and belonging to the plane $\langle O, \underline{b}_1, \underline{b}_2 \rangle$ identifies with the unit vector of the blade chord and it is given by

$$\frac{(P-C)^{\perp}}{|(P-C)^{\perp}|} = \frac{(-R\sin\theta + s\cos\beta)\underline{b}_1 + (R\cos\theta + s\sin\beta)\underline{b}_2}{\sqrt{(-R\sin\theta + s\cos\beta)^2 + (R\cos\theta + s\sin\beta)^2}} \tag{6}$$

The pivoting motion of the blade around its shaft can be characterized by the angle α (function of time) between the unit vectors $\underline{t}$ and $\frac{(P-C)^{\perp}}{|(P-C)^{\perp}|}$. Due to the relation

$$cos\alpha = \frac{(P-C)^{\perp}}{|(P-C)^{\perp}|} \cdot \underline{t} = \frac{R + s\sin(\beta - \theta)}{\sqrt{(-R\sin\theta + s\cos\beta)^2 + (R\cos\theta + s\sin\beta)^2}} \tag{7}$$

where the dot denotes the usual scalar product between vectors, the pivoting angle α can be defined as

$$\alpha = \begin{cases} \cos^{-1}\left(\dfrac{(P-C)^{\perp}}{|(P-C)^{\perp}|}\cdot \underline{t}\right) & \text{if } \cos(\theta-\beta) \geq 0 \\ -\cos^{-1}\left(\dfrac{(P-C)^{\perp}}{|(P-C)^{\perp}|}\cdot \underline{t}\right) & \text{otherwise} \end{cases} \tag{8}$$

choosing anticlockwise the positive direction of rotation around the blade shaft. The above outlined kinematical model can be summarized by Figure 1.

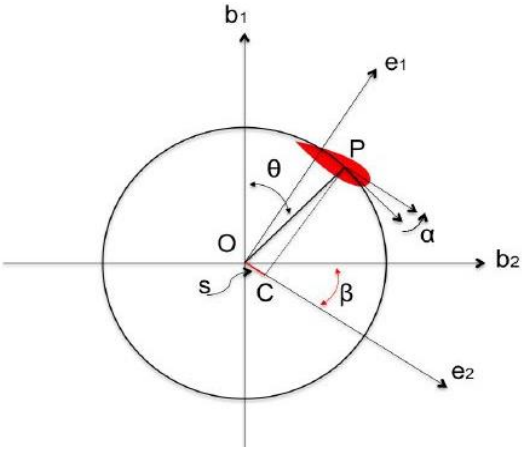

Figure 1: Kinematics of the blade

Supposing now that the vessel is moving, let $\underline{v}_O = \hat{u}\underline{b}_1 + \hat{v}\underline{b}_2$ be the velocity of O (w.r.t. the Earth-fixed frame) expressed in the hull-fixed basis. Denoting by $\underline{v}'_P = -R\dot{\theta}\, sin\,\theta\, \underline{b}_1 + R\dot{\theta}\, cos\,\theta\, \underline{b}_2$ the velocity of the point P w.r.t. the body-fixed frame, the velocity of P w.r.t. the Earth-fixed frame is given by

$$\underline{v}_P = \underline{v}'_P + \underline{v}_{\hat{O}} + \underline{\omega} \wedge (P-O) = \left[\hat{u} - R\left(\dot{\theta}+r\right)\sin\theta\right]\underline{b}_1 + \left[\hat{v} + R\left(\dot{\theta}+r\right)\cos\theta\right]\underline{b}_2 \tag{9}$$

where $\underline{\omega} = r\underline{b}_3$ is the angular velocity of the vessel. The velocity of the incoming flow experienced at P by a blade-fixed observer is, then $-\underline{v}_P$; its unit vector $\hat{\underline{t}}$ is expressed as

$$\hat{\underline{t}} = -\frac{\underline{v}_P}{|\underline{v}_P|} = -\frac{\left[\hat{u} - R\left(\dot{\theta}+r\right)\sin\theta\right]\underline{b}_1 + \left[\hat{v} + R\left(\dot{\theta}+r\right)\cos\theta\right]\underline{b}_2}{\sqrt{\left[\hat{u} - R\left(\dot{\theta}+r\right)\sin\theta\right]^2 + \left[\hat{v} + R\left(\dot{\theta}+r\right)\cos\theta\right]^2}} \tag{10}$$

Making use of the unit vector $\hat{\underline{t}}$, it is possible to characterize the attack angle of the incident flow as

$$\hat{\alpha} = \pi - \cos^{-1}\left[\frac{(P-C)^{\perp}}{|(P-C)^{\perp}|}\cdot \hat{\underline{t}}\right] \tag{11}$$

according to Figure 2.

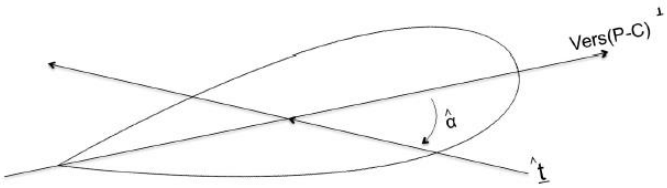

Figure 2: Angle of attack

2.2 Hydrodynamic forces

In this section, making use of some simplifying assumptions, a suitable model for evaluating the hydrodynamic forces generated by each blade is presented. It is supposed that the velocity of the incident flow be the same over the entire surface of the blade and coincide with $-\underline{v}_P$. Under such a condition, the lift and drag produced by each blade can be expressed as

$$\underline{L} = c_L \frac{1}{2}\rho_w A \left|\underline{v}_P\right|^2 \hat{\underline{n}} \qquad\qquad \underline{D} = c_D \frac{1}{2}\rho_w A \left|\underline{v}_P\right|^2 \hat{\underline{t}} \tag{12}$$

where c_L is the lift coefficient, c_D is the drag coefficient, ρ_w is sea water density, A is the blade lateral area, $\left|\underline{v}_P\right|$ is the incoming flow speed, $\hat{\underline{t}}$ is the unit vector of the lift force (unit vector of the incoming flow at P), and $\hat{\underline{n}}$ is the unit vector of the drag force (perpendicular to $\hat{\underline{t}}$).

In order to determine the unit vector $\hat{\underline{n}}$, the following procedure is adopted in which two main scenarios are distinguished:

- the attack angle $\hat{\alpha}$ belongs to the interval $\left]0, \frac{\pi}{2}\right[$, namely the incoming flow hits the blade from the front. In such a circumstance, the unit vector $\hat{\underline{n}}$ is determined according to the requirements:

$$\hat{\underline{n}} = \begin{cases} \underline{b}_3 \wedge \hat{\underline{t}} & \text{when } \hat{\underline{t}} \wedge \dfrac{(P-C)^{\perp}}{|(P-C)^{\perp}|} \cdot \underline{b}_3 > 0 \\ -\underline{b}_3 \wedge \hat{\underline{t}} & \text{when } \hat{\underline{t}} \wedge \dfrac{(P-C)^{\perp}}{|(P-C)^{\perp}|} \cdot \underline{b}_3 < 0 \end{cases} \tag{13}$$

- $\hat{\alpha} \epsilon \left]\frac{\pi}{2}, \pi\right[$, the incoming flow hits the blade from the back. In this case, $\hat{\underline{n}}$ is singled out by the requests:

$$\hat{\underline{n}} = \begin{cases} -\underline{b}_3 \wedge \hat{\underline{t}} & \text{when } \hat{\underline{t}} \wedge \dfrac{(P-C)^{\perp}}{|(P-C)^{\perp}|} \cdot \underline{b}_3 > 0 \\ \underline{b}_3 \wedge \hat{\underline{t}} & \text{when } \hat{\underline{t}} \wedge \dfrac{(P-C)^{\perp}}{|(P-C)^{\perp}|} \cdot \underline{b}_3 < 0 \end{cases} \tag{14}$$

As remaining particular cases, if $\hat{\alpha} = 0$ or $\hat{\alpha} = \pi$ there is no lift while if $\hat{\alpha} = \frac{\pi}{2}$ then $\hat{\underline{n}} = \hat{\underline{t}}$. The above described procedure allows to determine the lift and drag provided by each single

blade. The resultant hydrodynamic force generated by the cycloidal propeller can be computed as the sum of all contributions by each blade**.**

2.3 Torque acting on the rotor

The calculation of the torque acting on the rotor deserves a specific discussion. In order to accomplish this task, the Newton-Euler moment equation for each single blade has to be considered. Developed in the hull-fixed reference frame and with respect to the point O, the Newton-Euler moments equation for each blade can be expressed as

$$\underline{M}_O^E + \underline{M}_O^H + \underline{M}_O^G + \underline{M}_O^R + \underline{M}_O^I = I_G(\underline{\dot{\omega}}) + \underline{\omega} \wedge I_G(\underline{\omega}) + m(G-O) \wedge \underline{a}_G \tag{15}$$

where $\underline{M}_O^E$, $\underline{M}_O^G$, $\underline{M}_O^H$, $\underline{M}_O^R$, and $\underline{M}_O^I$ are the engine, hydrodynamic, weight force, reactive force, and inertial force torques w.r.t. O, respectively; I_G is the inertia tensor w.r.t. the center gravity G of the blade; $\underline{\omega}$ is the blade angular velocity w.r.t. the hull-fixed frame; $\underline{a}_G$ is the acceleration of G w.r.t. the hull-fixed frame; and m is the blade mass.

Knowing the revolution velocity of the rotor and the position of the steering center as well as the velocity of the incoming flow, the consequent motion of the blade is known from kinematics; at the same time, the knowledge of the hydrodynamic forces allows the evaluation of their moment. Neglecting the rolling friction around the rotation axis, the (scalar value of) engine torque amounts to the projection

$$M_O^E = -\underline{M}_O^H \cdot \underline{b}_3 - \underline{M}_O^I \cdot \underline{b}_3 + I_G(\underline{\dot{\omega}}) \cdot \underline{b}_3 + m(G-O) \wedge \underline{a}_G \cdot \underline{b}_3 \tag{16}$$

Once again, by adding all the contributions by each blade, the total engine torque can be obtained**.**

3 NUMERICAL MODELLING AND VALIDATION

The kinematical model has been used to develop a Matlab-Simulink simulator for cycloidal propellers. In this section, the main features and the validation of such simulator are presented.

3.1 Simplifying assumptions

In order to simplify the simulation platform, some hypotheses have been assumed:

- the propeller is considered in free-running conditions (no hull interference), as in open water, invested from an incoming flow;
- the problem is supposed to be stationary;
- the model is 2D;
- the contributions of each single blade are separately calculated and then summed. The interference among the blades is taken into account by means of correction factors.

3.2 Input data

The Simulink model needs input data, given from Matlab file. These data are: the geometry of the propeller (length, chord and orbit diameter of the blade – see Table 1); the sea water

characteristics (viscosity and density); the C_L and C_D coefficients of the blade (obtained by a previous CFD calculation [6]); the rotor speed and maximum pitch available; the steering pitch angle (0° in forward direction, 180° in astern condition) and the driving pitch (expressed as a percentage of the radius of the orbit of the blades).

Table 1: Propeller geometric parameters.

N. of blades	5
Diameter (m)	3.2
Blade length (m)	2.65
Blade Chord (m)	0.7744
Max tip thickness	0.242

3.3 Simulation

The simulator allows to generate the curves of the coefficients K_S and K_D, respectively defined by

Thrust Coefficient
$$K_S = \frac{T}{\frac{1}{2}\rho_w D L u^2} \tag{17.a}$$

Torque Coefficient
$$K_D = \frac{4M}{\rho_w D^2 L u^2} \tag{17.b}$$

and depending on the advance coefficient

$$\boldsymbol{\lambda = \frac{V_A}{\pi n D}} \tag{17.c}$$

where T is the total thrust, M is the total torque acting on the rotor , L is the blade height, and $u = \pi n D$ is the revolution speed of the blades.

The whole model consists of a set of identical subsystems, each of them representing the behaviour of a single blade. Making use of Eqs. (12) and (15), the components of total thrust and torque are calculated in the basis $\{\underline{b}_i\}$. According to Eqs. (17.a) and (17.b), it is then possible to evaluate the coefficients K_S and K_D. The simulation of coefficient K_S and K_D has been performed in the pitch range from 40% to 80%, with steps of 10%. In particular, Figure 3 shows the comparison between literature data (pertinent to a real existing cycloidal propeller, characterized by the same geometry) and the simulation of the coefficients K_S and K_D without any corrections for a pitch of 80%.

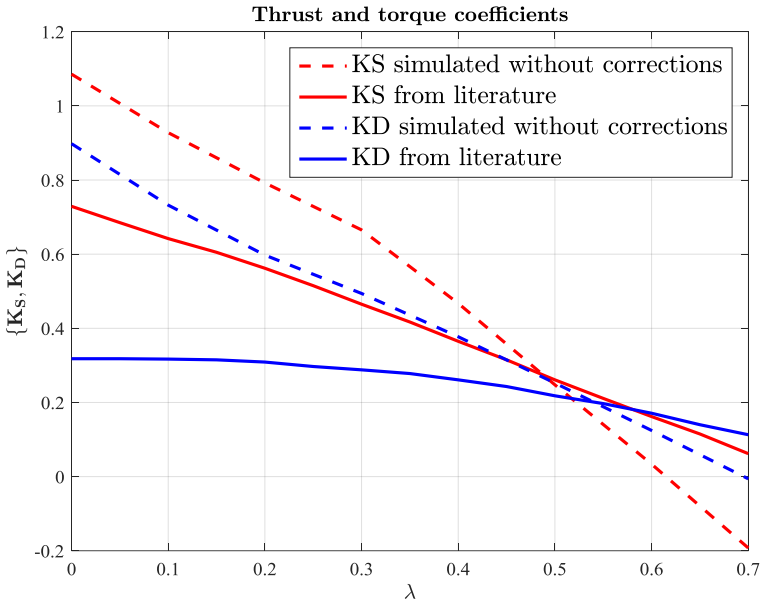

Figure 3: Thrust and torque coefficients of the cycloidal thruster.

3.4 Model validation

The differences shown in Figure 3 are mainly due to the stated simplifying assumptions about the interactions among the blades. In order to minimize these differences, two correction factors have been introduced, taking two main phenomena into account: the shielding of the blades that are in the half circumference not directly exposed to the incoming flow and the interference of a blade with the other. The calibration of such correction factors has been carried out by comparing simulation results with the performance data of the existing propeller. The comparison is shown in Figure 4.

Once the curves of K_S and K_D have been obtained, the total thrust for an advance coefficient of 0.4 and different thrust directions has been analysed. The numerical modelling showed a slight reduction of thrust magnitude for the reverse thrust. In order to consider this further phenomenon, another correction factor has been introduced, according to the existing propeller performance. The results are illustrated in Figure 5.

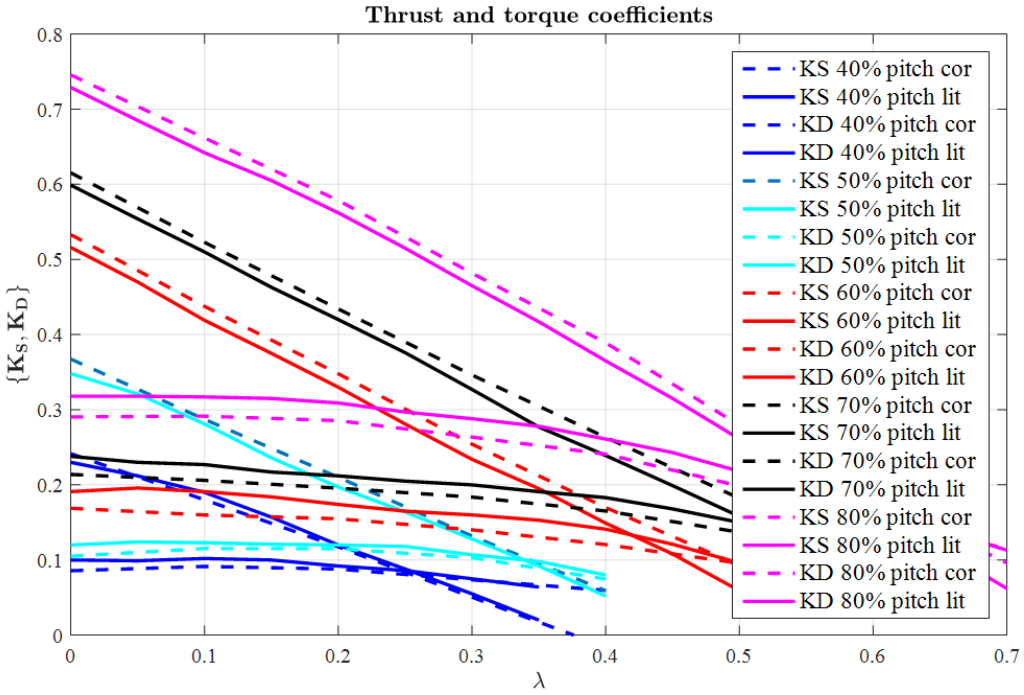

Figure 4: Thrust and torque coefficients of the cycloidal thruster.

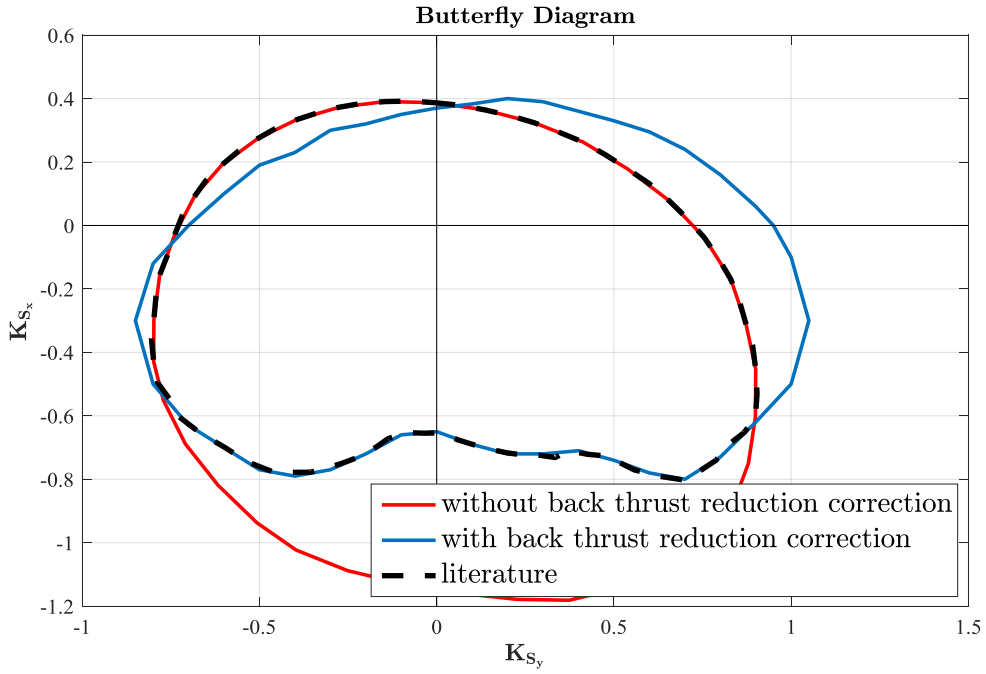

Figure 5: Thrust and torque coefficients of the cycloidal thruster.

Summarizing, the three considered corrections are:

- "Shielding correction", referring to the shielding of the blades that are in the half circumference not directly exposed to the incoming flow: in the model, the correction factor, depending on driving pitch values, reduces the velocity of the incoming water flow.
- "Interference correction": the interference among the blades is modelled by reducing the attack angle of the incoming flow in respect to the chord of the blade section; the correction depends on λ and pitch values.
- "Reverse thrust correction", representing the reduction of the reverse thrust.

The correction factors, empirically estimated for a particular propeller, are represented in terms of percentage reductions. In the case of cycloidal propellers with a different number of blades, the same correction values can be considered for an overall estimation of the propeller performance, achieving good results [7]; obviously, for a more reliable simulation, the correction factors have to be calibrated again for each particular application.

As it has been already mentioned, the main strength of the proposed simulation approach comes from not having to calculate the propeller fluid dynamics, avoiding demanding computations that would not allow an effective simulation of the whole propulsion plant.

As an application, the numerical model has been used for the performance evaluation of a DP system of a surface vessel equipped with two cycloidal propellers at the stern and a single bow thruster. The examined ship is the same for which a DP system, characterized by a conventional twin-screw propulsion, was already developed by the automation provider Seastema S.p.A. in cooperation with University of Genoa [5].

4 DYNAMIC POSITIONING APPLICATION

The first step in the assessment of the performance of a given dynamic positioning system is the evaluation of the static capabilities of the vessel. In order to accomplish this task, dynamic positioning polar plots are a useful tool. In the following, the DP polar plots for the vessel considered in our study are presented, taking two different allocation logics into account. Finally, comparisons with the DP capability of the real ship (equipped with a standard propulsion configuration) are reported.

4.1 Environmental disturbances

The analysis is performed in static conditions and involves the balancing of the forces and moments generated by environmental disturbances (selected from the world wide sea state table). Environmental disturbances are described as the sum of forces and moments due to wind, current and wave respectively. Forces and moments are expressed making use of the well-known resistance form, depending on non-dimensional coefficients $C_X(\gamma_r)$, $C_Y(\gamma_r)$, and $C_N(\gamma_r)$, related respectively to the longitudinal force, the lateral force and the moment. γ_r is the relative angle between the disturbance incoming direction and the vessel heading In order to consider the occurring worst condition, all environmental disturbances are supposed to be aligned in the same incoming direction, thus γ_r is the same for current, wind and waves. The

current and the wind speeds are assumed constant and wave drift forces are modelled as proportional to the square of the significant height H_s [5]. Collecting all the (b-basis) components of the force and moment in a unique 3-dimensional array τ, we have

$$\boldsymbol{\tau_E} = \boldsymbol{\tau_{current}}(\boldsymbol{\gamma_r}) + \boldsymbol{\tau_{waves}}(\boldsymbol{\gamma_r}, \boldsymbol{H_s}) + \boldsymbol{\tau_{wind}}(\boldsymbol{\gamma_r}, \boldsymbol{v_G}) \tag{18}$$

4.2 Thrust allocation logic

In order to assess the DP capability of the propulsion configuration with cycloidal propellers, two allocation logics have been developed and compared . with the one implemented on the real vessel, equipped with two traditional propellers and rudders. Details of the original allocation can be found in [5].

The first allocation logic is based on a constrained minimum problem . The idea is to minimize a cost function of seven variables $\underline{x} = [T_{pt}, T_{sb}, T_{bow}, X_{pt}, Y_{pt}, X_{sb}, Y_{sb}] \in \mathbb{R}^7$, subject to some suitable constraints. In particular, defining by T_{pt} and T_{sb} respectively the portside and starboard cycloidal propeller thrusts, T_{bow} the thrust of the bow thruster, (X_{pt}, Y_{pt}) and (X_{sb}, Y_{sb}) the components of the portside and starboard thrust forces, the constrained minimum problem is formulated as

$$\min_{\underline{x}} f(\underline{x}) \quad \text{with} \quad h_i(\underline{x}) = 0 \quad \text{and} \quad g_j(\underline{x}) > 0 \tag{19}$$

where

$$f(\underline{x}) = \left(\frac{T_{pt}}{T_{max}^{tot}}\right)^2 + \left(\frac{T_{sb}}{T_{max}^{tot}}\right)^2 + \left(\frac{T_{bow}}{T_{max}^{tot}}\right)^2 \tag{20}$$

is the cost function to be minimized, and

$$\begin{cases} h_1(\underline{x}) = X_{env} - X_{pt} - X_{sb} \\ h_2(\underline{x}) = Y_{env} - Y_{pt} - Y_{sb} - T_{bow} \\ h_3(\underline{x}) = N_{env} - x_{bow}\ T_{bow} - x_{pt}\ Y_{pt} + \\ \qquad\qquad + y_{pt}\ X_{pt} - x_{sb}\ Y_{sb} + y_{sb}\ X_{sb} \\ h_4(\underline{x}) = T_{pt}^2 - X_{pt}^2 - Y_{pt}^2 \\ h_5(\underline{x}) = T_{sb}^2 - X_{sb}^2 - Y_{sb}^2 \end{cases} \tag{21}$$

are the constraints to be satisfied. In Eq. (21) $\{X_{env}, Y_{env}, N_{env}\}$ are the components of the force and the moment due to environmental disturbances, (x_{pt}, y_{pt}) and (x_{sb}, y_{sb}) are the coordinates of the propellers thrust centres and x_{bow} is the longitudinal coordinate of the bow thruster. Moreover, we have

$$g_1(\underline{x}) = x(2) \quad , \quad g_2(\underline{x}) = x(3) \tag{22}$$

Eq. (19) requires that the sum of the squared desired thrusts is minimum. Eq.(21) details the constraints: the first three represent the static equilibrium between the environmental disturbances and the delivered force and moment; the last two correlate the portside and

starboard thrust force with their longitudinal and lateral components. Finally, Eq. (22) ensures that the modulus of the two aft thrusts is positive.

The second allocation algorithm is based on the idea that one cycloidal propeller is designed to compensate the environmental resultant force, while the other one together with the bow thruster, is devoted to compensate the moment. This allocation configuration is supposed to be more stable when environmental disturbances are relatively small and constant in time. In this case, the force and moment balance is uniquely determined in an algebraic way, whenever the thruster devoted to the force compensation is chosen. The choice of such a thruster relies on the requirement that the moment generated by the thruster itself has opposite sign with respect to the disturbances one. More explicitly, we have

$$\begin{aligned} T_i &= \sqrt{X_{env}^2 + Y_{env}^2} \quad , \quad \delta_i = \tan^{-1}\frac{Y_{env}}{X_{env}} \\ T_{bow} &= -T_j \\ T_j &= \frac{x_i\, T_i \sin\delta_i \; - y_i T_i \cos\delta_i + N_{env}}{x_j - x_{bow}} \end{aligned} \tag{23}$$

where $i = pt$ and $j = sb$ when $\left|N_{pt} - N_{env}\right| > |N_{sb} - N_{env}|$ and $i = sb$ and $j = pt$ otherwise; N_{pt} is the moment generated by the propeller if portside is the one compensating the force and viceversa for N_{sb}.

The criterion adopted to choose the thrust devoted to compensate the disturbances force is based on computing, for both the possible choices, the moment generated by the thruster and adding it to the environmental one. Such resulting moments are compared and the thruster generating the minimum moment is the one chosen for the environmental force compensation.

4.3 Results

The station keeping capability of a dynamically positioned vessel is often presented by means of polar plots, which illustrate the steady-state performance of the vessel under certain environmental conditions. A capability plot shows the maximum weather conditions in which the vessel can maintain its position and heading, obeying upon a certain thrust allocation logic. DP capability plots are drawn assuming that the all environmental disturbances come from the same direction. In this case study, the vessel is supposed to operate in Mediterranean Sea with a significant wave height H_s of $2.5\,m$ and a constant current speed v_G of $1kn$. Instead, the wind speed keeps increasing until the vessel is able to sustain the wind load, namely until the resultant environmental forces and moments are balanced by the maximum available thrust. Assuming that the aligned environmental disturbances rotate around the vessel (anticlockwise starting from zero which corresponds to stern), in Figure 6 the intersection of the curve with the radius of the circumference indicates the maximum wind speed at which the vessel can maintain its position and heading. For reasons of readability of the plot, a saturation was added when the maximum wind speed was higher than 60kn. Moreover, higher wind conditions involves sea disturbances that cannot be studied in the static case.

As it can be seen in Figure 6, maximum values of wind speed can be reached for disturbances coming from bow directions, while we have lower values for beam and stern directions. That is due to the larger areas exposed to the environmental loads. Regarding the differences due to the distinct propulsion configurations, numerical results show that the conventional propulsion layout is able to ensure only a limited DP capability (the yellow line), while great improvements could come from the adoption of cycloidal propellers in the propulsion system. Concerning the different allocation logics adopted for cycloidal propellers, it is evident that the optimization of the thrust (the red line) gives the best results, though this is mainly true for bow and quartering sea states, while for stern sea states the two allocation logics seem to give closer results.

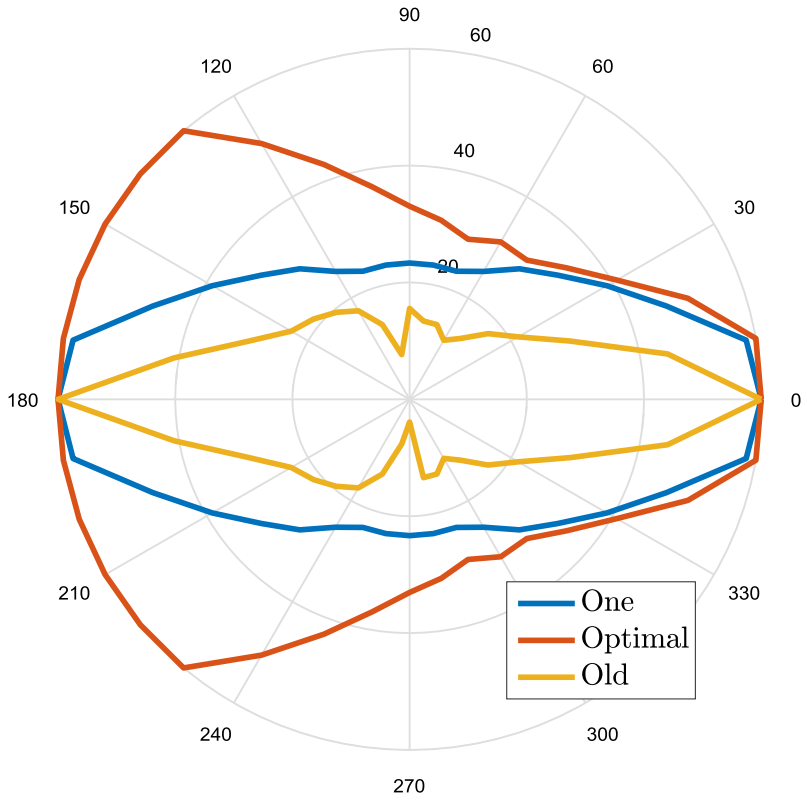

Figure 6: DP capability polar plots for different thrust allocation logics.

8 CONCLUSIONS

A simulation model for ship cycloidal propellers has been presented. The simulator has been calibrated by comparing simulation data with experimental ones. The mathematical and numerical modelling of the free running behaviour of cycloidal propellers, in different operating conditions, is described without using a proper - but also demanding - fluid dynamics computation (CFD method is only used for the evaluation of the lift and drag coefficients of the single blade).

The core of the model is represented by the kinematical description and by the empirical correction factors that can be used for a preliminary performance estimation of several cycloidal propulsion units, characterized by different lengths and number of blades.

In this light, the performance analysis of the DP application shown in this study can represent a possible proper application of the developed propulsion model. In particular, a comparison between a traditional propulsion system and the cycloidal one has been carried out in terms of DP capability plots. Further considerations, in terms of comparison, could be made also in case of different cycloidal units, by changing blades area and number.

The present work aims to be the first step towards the implementation of a numerical model for the dynamical simulation of the manoeuvrability, at both low and high velocities, of vessels equipped with cycloidal propellers.

REFERENCES

[1] Bose, N. *Marine Powering Prediction and Propulsors*. The Society of Naval Architects and Marine Engineers (2008).

[2] Jürgens, D. and Moltrecht, T. Enhanced cycloidal propulsion. *The International Workboat Show*, New Orleans (2002).

[3] Altosole, M., Benvenuto, G., Figari, M. and Campora, U. Dimensionless Numerical Approaches for the Performance Prediction of Marine Waterjet Propulsion Units. *Int. J. Rotat. Mach.* (2012) Article ID 321306.

[4] Taniguchi, K. Sea Analysis of the vertical axis propeller. *Proc. of the 4th symposium on Naval Hydrodynamics*, Office of Naval Research, Washington (1962).

[5] A. Alessandri, R. Chiti, S. Donnarumma, G. Luria, M. Martelli, L. Sebastiani and S. Vignolo. Dynamic Positioning system of a vessel with conventional propulsion configuration: Modeling and Simulation, Proceedings of Martech 2014, 2ND International Conference on Maritime Technology and Engineering, Lisbon, Portugal, 15-17 October 2014, pp – 725-733.

[6] Canaccini, C. and Canepa, F. Numerical simulation approach for the performance assessment of a cycloidal propeller. *Master degree thesis*, University of Genoa, Italy (2013).

[7] Battistoni, L. Numerical simulation approach for the preliminary design of a cycloidalpropeller. Master degree thesis, University of Genoa, Italy (2014).